This article was downloaded by:
On: *25 January 2011*
Access details: *Access Details: Free Access*
Publisher *Taylor & Francis*
Informa Ltd Registered in England and Wales Registered Number: 1072954 Registered office: Mortimer House, 37-41 Mortimer Street, London W1T 3JH, UK

Liquid Crystals
Publication details, including instructions for authors and subscription information:
http://www.informaworld.com/smpp/title~content=t713926090

Three-dimensional switchable polymer photonic crystals via various optical wave interference techniques

Gregory R. Yandek[a]; Scott[a]; Grigori M. Sigalov[a]; Thein Kyu[a]
[a] Institute of Polymer Engineering, The University of Akron, Akron, OH 44325

To cite this Article Yandek, Gregory R. , Scott, Sigalov, Grigori M. and Kyu, Thein(2006) 'Three-dimensional switchable polymer photonic crystals via various optical wave interference techniques', Liquid Crystals, 33: 7, 775 — 788
To link to this Article: DOI: 10.1080/02678290600722981
URL: http://dx.doi.org/10.1080/02678290600722981

PLEASE SCROLL DOWN FOR ARTICLE

Full terms and conditions of use: http://www.informaworld.com/terms-and-conditions-of-access.pdf

This article may be used for research, teaching and private study purposes. Any substantial or systematic reproduction, re-distribution, re-selling, loan or sub-licensing, systematic supply or distribution in any form to anyone is expressly forbidden.

The publisher does not give any warranty express or implied or make any representation that the contents will be complete or accurate or up to date. The accuracy of any instructions, formulae and drug doses should be independently verified with primary sources. The publisher shall not be liable for any loss, actions, claims, proceedings, demand or costs or damages whatsoever or howsoever caused arising directly or indirectly in connection with or arising out of the use of this material.

Liquid Crystals, Vol. 33, No. 7, July 2006, 775–788

Taylor & Francis
Taylor & Francis Group

Three-dimensional switchable polymer photonic crystals via various optical wave interference techniques

GREGORY R. YANDEK, SCOTT MENG, GRIGORI M. SIGALOV and THEIN KYU*
Institute of Polymer Engineering, The University of Akron, Akron, OH 44325, USA

(*Received 1 December 2005; accepted 19 January 2006*)

A theoretical study has been undertaken to elucidate the three-dimensional pattern formation during holographic polymer-dispersed liquid crystal fabrication employing various optical wave interference techniques. Initially miscible mixtures of nematic liquid crystal and reactive multifunctional monomer with a photosensitive initiator were exposed to geometrically arranged interfering beams of light, producing a spatially dependent intensity distribution within the sample. To mimic the spatio-temporal evolution of periodic photonic structures in three dimensions, the time-dependent Ginzburg–Landau Model C equations, coupled with spatially variant reaction rate equations, have been solved numerically incorporating the local free energy densities pertaining to isotropic mixing, nematic ordering, and network elasticity. The simulated results reveal some key observations during the formation of electrically switchable photonic crystals with few defects. It appears that the network elasticity term exerts profound effects on resultant structures, indicating that photonic crystals with fewer point defects may be fabricated in shorter times. The simulated results are in good qualitative agreement with reported experimental observations in respect of emerged patterns, length and time scales.

Downloaded At: 15:58 25 January 2011

1. Introduction

Photonic crystals are essentially materials exhibiting a photonic band gap (PBG). They have been so-named in view of the analogy that forbidden photon bands have an energy gap that electrons experience in semiconductor crystals [1]. This technology allows the control of photons such that certain wavelengths of light, defined by the structure of the crystal, are obstructed from propagating through the dielectric material. There has been immense interest in the past decade with regard to the fabrication of these materials since the realization that such structures afford the transition towards the increasingly advanced technologies of telecommunications and massive data storage, a field that is expected to grow for many years to come. Although electronic integrated circuits remain dominant in the current information technology market, there is an increasing demand for the advancement of photonic technology to develop the next generation of photonic integrated circuits.

Photonic crystals may be classified as one-, two-, or three-dimensional depending on their inherent periodicities. These structures generally consist of materials possessing a high dielectric constant in contrast with air. Numerous techniques have been developed for their fabrication, namely mechanical drilling [2], high resolution lithography [3], and colloidal self-assembly [4]. Semi conducting materials such as silicon and gallium arsenide are excellent candidates for photonic crystal fabrication as these materials possess high refractive indices and low absorptions, potentially exhibiting full band gaps in two and three dimensions. Polymers, on the other hand, maintain much lower refractive indices than the aforementioned inorganic materials, and although they do not possess a full potential photonic band gap, are interesting and viable candidates in switchable photonic crystal fabrication. Several different techniques have been utilized in the construction of polymer-based photonic crystals, including (1) the two-photon polymerization of photoresists in the generation of woodpile structures [5]; (2) the self-assembly of block copolymer or colloidal crystal systems revealing crystals with periodicities in one, two, and three dimensions [6–8]; and (3) the formation of holographic polymer-dispersed liquid crystalline (H-PDLC) materials via pattern photopolymerization [9, 10], alternatively known as the holographic lithography technique [11], which is the focus of the theoretical treatment in this paper.

H-PDLC materials formed by pattern photopolymerization are attractive in photonic applications, because

*Corresponding author. Email: tkyu@uakron.edu

Liquid Crystals
ISSN 0267-8292 print/ISSN 1366-5855 online © 2006 Taylor & Francis
http://www.tandf.co.uk/journals
DOI: 10.1080/02678290600722981

of their rapid fabrication times (of the order of seconds), and the tunable (or switchable) nature of the liquid crystal director orientation through the application of external electric fields. Pattern photopolymerization is a preferred technique for the fabrication of H-PDLC, where an initially miscible mixture of photocurable monomer, nematic liquid crystal, and photosensitive initiator is exposed to multiple geometrically arranged light beams interfering at the sample surface to activate the initiator, triggering polymerization. The mixing of incoming waves gives rise to constructive and destructive interference (wave mixing), producing regions of high and low intensity within the material. Polymerization occurs predominantly in regions of high intensity, and the resulting molecular mass increase shifts the coexistence curves asymmetrically up, thrusting the mixture from an initially miscible state into an immiscible gap. Monomers in regions of low intensity diffuse into regions of high intensity to become polymerized; in the same way, LC molecules diffuse from regions of high intensity into regions of low intensity.

The majority of studies concerning the formation of H-PDLC have utilized two or more beams for hologram writing, yielding structures consisting of micro-channel layers and/or micro-droplet arrays of liquid crystal between polymer-rich layers, structures which may be classified as one-dimensional or two-dimensional photonic crystals [11–15]. Such periodic structures (diffraction gratings) containing LC have a unique character, in that upon application of an external electric field their optical properties may be tuned. The successful applications of these photonic structures in telecommunication, specifically as transmission gratings, rely on the refractive index mismatch between the polymer rich stripe and the LC rich stripe, such that incident beams are diffracted. Once the grating is subjected to an applied voltage, the LC molecules orient themselves in the direction of the field, causing the overall ordinary refractive index of the system to match with the average refractive index of the surrounding matrix, permitting the incident beam to transmit without diffraction.

The optical properties of H-PDLC materials such as diffraction efficiency, switching voltages, and response times are heavily influenced both by the emerged morphologies from the pattern photo-polymerization process as well as the material selection. The emerging morphologies are determined strictly by the interplay between the photoreaction rates and phase separation dynamics of the system, which are rooted in the governing thermodynamics of the materials involved. Modelling techniques afford insights into the underlying physics of the pattern-forming process, revealing how structures may be optimized without the expense of extensive experimental trial-and-error approaches. Although there have been numerous theoretical efforts with various schemes by our group amongst others [16–24], the aim of this work is to extend the knowledge on the topic utilizing the traditional theoretical framework proposed by our group [22, 23], particularly in paying special attention to the elastic free energy contribution from the cross-linked network, so that optimal structures may be achieved. Another purpose of this paper is to illustrate the generation of various types of photonic crystals by altering the configuration of the writing beams.

2. Model development and simulation scheme

2.1. *Model description*

The mixture under consideration consists of nematic liquid crystal as well as multifunctional photoreactive monomer. As the photoreaction kinetics is very fast, the initial conversion of monomer to polymer is considered nearly instantaneous. However, the reaction rate constant, after the initial instantaneous rise, may decline with continued elapsed time in a manner dependent on the light intensity and concentration of liquid crystal.

In the context of the theoretical treatment previously proposed and utilized by our group [22, 25], the pattern formation aspects of the photopolymerization-induced phase separation process may be elucidated through the evolution of concentration and orientation order parameters of the time-dependent Ginzburg–Landau TDGL (Model C) equations as follows [26]:

$$\frac{\partial \phi_{\mathrm{LC}}(\mathbf{r}, t)}{\partial t} = \nabla \cdot \left[\Lambda \nabla \left(\frac{\delta G}{\delta \phi_{\mathrm{LC}}} \right) \right] + \eta_{\mathrm{LC}} \tag{1}$$

$$\frac{\partial s(\mathbf{r}, t)}{\partial t} = -R_{\mathrm{s}} \left(\frac{\delta G}{\delta s} \right) + \eta_{\mathrm{s}} \tag{2}$$

where $\phi_{\mathrm{LC}}(\mathbf{r}, t)$ represents the conserved LC volume fraction (concentration order parameter) at position $\mathbf{r}$ and time t, while $s(\mathbf{r}, t)$ is the non-conserved LC orientation order parameter at the same position and time. The term R_{S} in equation (2) is related to the rotational mobility, which is taken as a constant for simplicity [27]. The total free energy of the system is represented by G, where $\delta/\delta s$ in equations (1, 2) is the functional derivative operator. The η terms in equations (1, 2) correspond to thermal noise in their respective fields, which satisfy the fluctuation-dissipation theorem [28]. The order parameters pertaining to the monomer and polymer volume fractions

Downloaded At: 15:58 25 January 2011

coupled with photopolymerization reaction terms may be expressed in the following forms:

$$\frac{\partial \phi_{\mathrm{M}}(\mathbf{r}, t)}{\partial t} = \nabla \cdot \left[\Lambda \nabla \left(\frac{\delta G}{\delta \phi_{\mathrm{M}}} \right) \right] - \frac{\mathrm{d}\alpha}{\mathrm{d}t} \phi_{\mathrm{M}} \tag{3}$$

$$\frac{\partial \phi_{\mathrm{P}}(\mathbf{r}, t)}{\partial t} = - \frac{\mathrm{d}\alpha}{\mathrm{d}t} \phi_{\mathrm{M}} \tag{4}$$

where the term $\mathrm{d}\alpha/\mathrm{d}t$ represents the rate of monomer conversion to polymer during the course of the photopolymerization. For the purposes of the present simulation, the system is assumed to be incompressible, such that the summation of the three individual volume fractions is always unity.

In equations (1) and (3), Λ is the mutual translational diffusion coefficient having the property of Onsager reciprocity defined as follows [25, 29]:

$$\Lambda = \frac{\Lambda_{\mathrm{M}} \Lambda_{\mathrm{LC}} + \Lambda_{\mathrm{M}} \Lambda_{\mathrm{P}} + \Lambda_{\mathrm{LC}} \Lambda_{\mathrm{P}}}{\Lambda_{\mathrm{M}} + \Lambda_{\mathrm{LC}} + \Lambda_{\mathrm{P}}}. \tag{5}$$

In the crosslinked polymer network, macromolecular chains may undergo local vibration or rotational motion, but there is virtually no translational mode of mobility, i.e. no molecular transport as the chains are practically anchored at the chemical junctions. Hence, one may approximate that $D_{\mathrm{p}}=0$, and thus $\Lambda_{\mathrm{P}}=0$. In equation (5), $\Lambda_{\mathrm{M}}=\phi_{\mathrm{M}} D_{\mathrm{M}}$ and $\Lambda_{\mathrm{LC}}=\phi_{\mathrm{LC}} D_{\mathrm{LC}}$. D_{M} and D_{LC} represent the self-diffusion coefficients of monomer and liquid crystal, respectively. The reader may note that the mobility of individual components (LC and monomer) is devoid of molecular mass terms, which are taken as unity since both constituents are monomers.

The total free energy of the system, G, may be expressed as [26]:

$$G = \int_V \left[g(\phi_{\mathrm{LC}}, \phi_{\mathrm{M}}, \phi_{\mathrm{P}}, s) + \kappa_\phi |\nabla \phi_{\mathrm{LC}}|^2 + \kappa_s |\nabla s|^2 \right] \mathrm{d}V \tag{6}$$

where g is the local free energy of the system, and the terms $\kappa_\phi |\nabla \phi_{\mathrm{LC}}|^2$ and $\kappa_s |\nabla s|^2$ are non-local terms associated with the gradients of the LC concentration and orientation order parameters, respectively. Within the non-local terms are κ_ϕ and κ_S which are gradient coefficients of their respective field, and κ_S is taken as a constant for simplicity in the calculations in the range used by others [25, 30, 31]. On the other hand, κ_ϕ may be determined from the following relation for an asymmetric mixture [32]:

$$\kappa_\phi = \frac{1}{36} \left[\frac{a_{\mathrm{LC}}^2}{\phi_{\mathrm{LC}}} + \frac{a_{\mathrm{M}}^2}{(1-\phi_{\mathrm{LC}})} \right] \tag{7}$$

where a_{LC} and a_{M}, are the characteristic lengths of the LC and monomeric units, respectively. For a symmetric blend $a_{\mathrm{LC}}=a_{\mathrm{M}}$, and equation (1) may be rewritten:

$$\frac{\partial \phi_{\mathrm{LC}}(\mathbf{r}, t)}{\partial t} = \nabla \cdot \left\{ \Lambda \nabla \left[\begin{array}{l} \frac{\delta G}{\delta \phi_{\mathrm{LC}}} + \frac{a_{\mathrm{LC}}^2 (1-2\phi_{\mathrm{LC}})}{36 \phi_{\mathrm{LC}}^2 (1-\phi_{LC})^2} (\nabla \phi_{\mathrm{LC}})^2 \\ - \frac{a_{\mathrm{LC}}^2 \nabla^2 \phi_{\mathrm{LC}}}{18 \phi_{\mathrm{LC}} (1-\phi_{LC})} \end{array} \right] + \kappa_s |\nabla s|^2 \right\}. \tag{8}$$

The local free energy density comprises three terms, namely the isotropic mixing (g^i), nematic ordering (g^n), and elastic (g^e) free energy densities as follows:

$$g = g^{\mathrm{i}} + g^{\mathrm{n}} + g^{\mathrm{e}}. \tag{9}$$

The free energy density of isotropic mixing may be expressed according to the Flory–Huggins theory by the following expression [33, 34]:

$$g^{\mathrm{i}} = \phi_{\mathrm{LC}} \ln \phi_{\mathrm{LC}} + \phi_{\mathrm{M}} \ln \phi_{\mathrm{M}} + \frac{\phi_{\mathrm{P}} \ln \phi_{\mathrm{P}}}{N_{\mathrm{P}}} + \chi \phi_{\mathrm{LC}} (1-\phi_{\mathrm{LC}}) \tag{10}$$

where N_{P} represents the chain length of the polymer and χ is the interaction parameter between the liquid crystal and the monomer/emerging polymer, assuming that the monomer and emerging polymer are miscible.

The free energy density of nematic ordering according to Maier–Saupe theory is given as follows [35]:

$$g^{\mathrm{n}} = \frac{1}{r_{\mathrm{LC}}} \left(- \phi_{\mathrm{LC}} \ln z + \frac{1}{2} v \phi_{\mathrm{LC}}^2 s^2 \right). \tag{11}$$

Here v represents the nematic interaction parameter of the form $v=4.541 T_{\mathrm{NI}}/T$, where T_{NI} is the liquid crystal nematic–isotropic transition temperature. The terms z and s are the normalized partition function and nematic order parameter, respectively, further expressed by the following integral forms [36]:

$$z = \int_0^1 \exp \left[\frac{v \phi_{\mathrm{LC}} s}{2} \left(3x^2 - 1 \right) \right] \mathrm{d}x \tag{12}$$

$$s = \frac{\int_0^1 \frac{1}{2} \left(3x^2 - 1 \right) \exp \left[\frac{v \phi_{\mathrm{LC}} s}{2} \left(3x^2 - 1 \right) \right] \mathrm{d}x}{z} \tag{13}$$

where $x=\cos\theta$, θ being the angle between the LC director and the reference axis.

An important goal of this paper is to investigate the role of the elastic free energy contribution from the emerging polymer network on the final structure of H-PDLC materials. The elastic free energy for a flexible crosslinked polymer chain that obeys ideal Gaussian chain statistics may be described according to the Dusek

Downloaded At: 15:58 25 January 2011

approach [37]:

$$g^e = \frac{3\alpha_e}{2r_c}\Phi_0^{2/3}\left(\phi_P^{1/3} - \phi_P\right) + \frac{\beta_c}{r_c}\phi_P \ln \phi_P \qquad (14)$$

where α_e and β_e are network constants. The term r_c is the segment length between crosslink points, which is related to the monomer conversion, α, as [38]

$$r_c = \frac{\alpha}{2-\alpha-2(1-\alpha)^{\frac{1}{2}}} . \qquad (15)$$

It is clear from this relationship that as the conversion increases, the segment length between crosslink points decreases, implying an increase in the crosslink density of the network.

Due to the difference of monomer type and curing kinetics in reality, the network constants in equation (14) may take assorted forms [39–41], and we have chosen those presented by Flory and Erman [42] in their junction fluctuation theory, allowing the constants to vary linearly with ϕ_P. Following the aforementioned theoretical treatment, those constants are defined as follows:

$$\alpha_e = (f-2)/f; \qquad \beta_e = 2\phi/f \qquad (16)$$

where the parameter f denotes the functionality of the crosslinks, taken as 3 in our calculations. The parameter Φ_0 in equation (14) represents the reference volume fraction of the polymer network. We set $\Phi_0 = \phi_P$, the volume fraction at the onset of crosslinking, in this work.

Considering the free radical essence of photopolymerization, the rate of monomer conversion to polymer during photopolymerization may be described for the purposes of this study by a first order kinetic equation of the form [43]

$$\frac{d\alpha}{dt} = k(1-\alpha) \qquad (17)$$

where t is the time and k is the apparent reaction rate constant with the units of reciprocal time. In actual photopolymerization, the rate constant k is dependent on the absorbed incident light intensity and reaction rate constants of propagation and termination. The value of k tends to change with reaction time, thus equation (17) is more complicated than the simplified first order kinetic expression. Since the experimental k can be readily determined from photodifferential scanning calorimetry (P-DSC) or Fourier transform infrared spectroscopy (FTIR), the experimental k value may be used in the simulation. The holographic aspects of the polymerization, i.e. the spatial distribution of light intensity within the sample, will be discussed in the following section.

2.2. *Numerical calculation procedure*

When modelling the spatio-temporal evolution of concentration order parameter of a LC in three dimensions, equations (1–4) are numerically solved on a lattice of dimensions $128 \times 128 \times 38$, coupled with the remaining equations described in the previous section. A finite difference method has been chosen for the spatial step, utilizing a central difference discretization scheme. An explicit method was utilized for the time step. Mixed boundary conditions were employed in the simulation to mimic the actual experimental conditions. The simulation size in the z-direction, representing the thickness, is taken to be of the order of actual samples used in experiments made by sandwiching the monomer/liquid crystal/photoinitiator solution between glass plates [11, 14]. Since the film thickness is significantly smaller than the two other dimensions in actual samples, periodic boundary conditions are imposed along the vertical boundaries (i.e. x- and y-dimensions). On the other hand, the z-direction represents the entire sample thickness and no-flux boundary conditions are imposed accordingly, as the glass plates that sandwich the sample are impermeable. The reference system for simulation is a typical multifunctional photoreactive monomer (e.g. triacrylate, tetracrylate) and nematic liquid crystal (e.g. E7). The diffusion coefficients are purposely chosen to stay in the experimental diffusion coefficient range for liquid crystal (10^{-7}–$10^{-8}\,cm^2\,s^{-1}$) and for multifunctional acrylic monomer (10^{-10} –$10^{-12}\,cm^2\,s^{-1}$), which will be elaborated on in a later section.

3. Results and discussion

3.1. *Phase diagrams of LClmonomer and LClpolymer mixtures*

The starting mixture of LC and photoreactive monomer is a binary system. Since the H-PDLC formation process is generally initiated in the isotropic region, construction of a phase diagram is an essential first step for undertaking numerical modelling. The conditions for equilibrium in nematic–isotropic phase separation for a binary system are

$$\mu_1\left(\phi_n^{\alpha}, s\right) = \mu_1\left(\phi_i^{\beta}, 0\right) \text{ and } \mu_2\left(\phi_n^{\alpha}, s\right) = \mu_2\left(\phi_i^{\beta}, 0\right) \qquad (18)$$

where μ_1 and μ_2 denote the chemical potentials of component 1 and 2 in both phases, determined by taking the partial derivatives of the free energy, G, with respect to the number of moles of that species. The theoretical phase diagram has been established previously by Meng *et al.*, showing a teapot phase diagram in which an upper critical solution temperature (UCST)

Downloaded At: 15:58 25 January 2011

is overlapped with the nematic–isotropic transition of the constituent LC, see figure 1 (*a*) [44]. The critical LC volume fraction is approximately located at 0.5, owing to the comparable sizes of the monomer and LC species, ($N_M=N_{LC}=1$), the critical temperature $T_c=27^\circ$C, and $T_{NI}=60^\circ$C, in accordance with experimental observation of the reference nematic liquid crystal. The dashed line in figure 1 (*a*) is the peritectic line separating isotropic–isotropic phase separation and liquid–nematic phase separation regions. I and N stand for isotropic and nematic, respectively, while m and u represent metastable and unstable, respectively.

Once photopolymerization is initiated, the mixture becomes a ternary system consisting of the emerging polymer, residual monomer and LC. For simplicity, the emerging polymer and residual monomers are assumed to be miscible so that the LC/monomer (or polymer) system under consideration can be treated as pseudo-binary. Snapshots of how the UCST coexistence curve of the starting mixture moves asymmetrically to elevated temperatures may be witnessed during the course of photopolymerization. Figure 1 (*b*) illustrates snapshots of the phase diagram with the progression of reaction time. The asymmetrical upward shift in the phase diagram is caused by the increase in length of the growing polymer species, resulting in a decrease in the entropic contribution to the free energy of the isotropic mixing, thereby expanding the unstable region of the phase diagram. In these calculations, the starting mixtures are at a temperature of 30°C in the initial isotropic region of the phase diagram, figure 1 (*a*).

As can be shown in the Flory–Huggins theory, the free energy of isotropic mixing changes drastically with increasing degree of polymerization. That is to say, photopolymerization increases the chain length of the polymeric constituent, thereby reducing the entropy of mixing which favours demixing as the system becomes unstable. This behaviour is depicted in figure 2, where it can be seen that in the initial state of the system (when $N_M=1$), the blend is stable against phase separation. However, as the polymerization advances to $N_M=10$ and beyond, the system becomes increasingly unstable, triggering phase separation into LC-rich and polymer-rich phases. It should be mentioned, however, that these

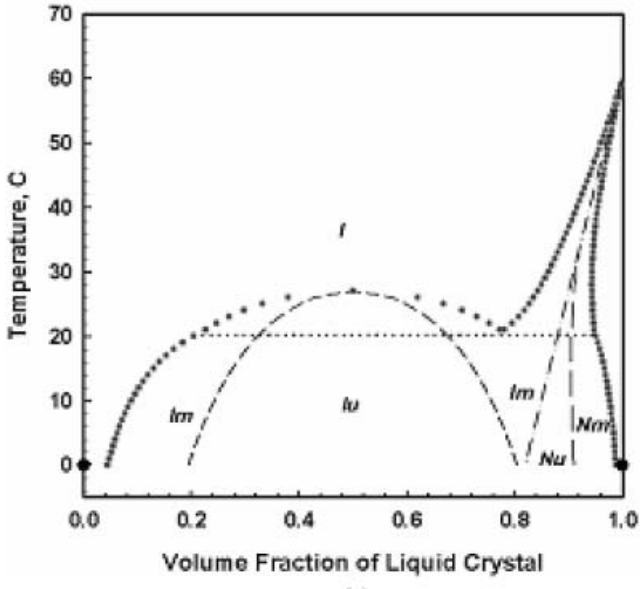

Figure 1. (*a*) Calculated initial phase diagram of liquid crystal/monomer mixture; (*b*) temporal evolution of the phase diagram during polymerization.

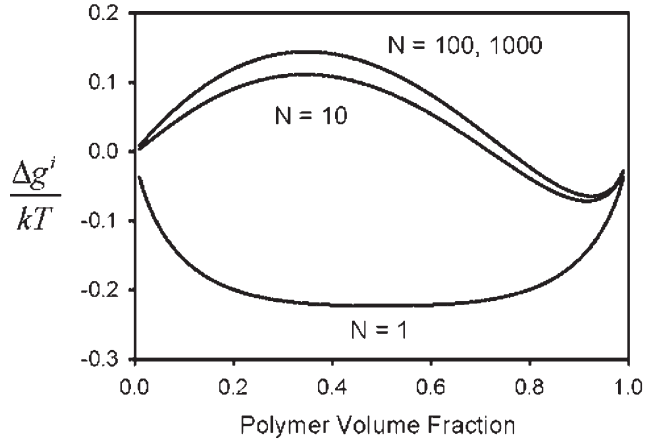

Figure 2. Change in the free energy of isotropic mixing as the statistical chain length of the polymer increases according to the Flory–Huggins theory.

Downloaded At: 15:58 25 January 2011

systems hardly reach equilibrium, especially when the photopolymerization proceeds so rapidly.

3.2. *Dynamics of pattern photopolymerization-induced phase separation (two-beam interference)*

To illustrate the dynamics of the pattern photopolymerization process, we first consider the traditional two-beam se-tup depicted in figure 3 (*a*), where the beams are positioned from opposite directions at an angle α from the normal to the sample surface. Structures generated by this optical configuration may be classified as one-dimensional photonic crystals. For the purposes of modelling, the incident light beams are considered to be coherent, possessing identical polarization and no phase difference. This modelling requires mathematical description of the interference patterns generated by the aforementioned wave mixing. To achieve this, the concept of the superposition of waves is employed [45, 46]. The irradiance figure for the two-beam light configuration is readily derived as follows:

$$\frac{I}{I_0} = 4\cos\left(\frac{N_x}{L}x\right)^2. \tag{19}$$

Here, x is the spatial location on the sample along the horizontal axis, I_0 is the maximum intensity. The term N_x/L in equation (19) is often referred to as the

Downloaded At: 15:58 25 January 2011

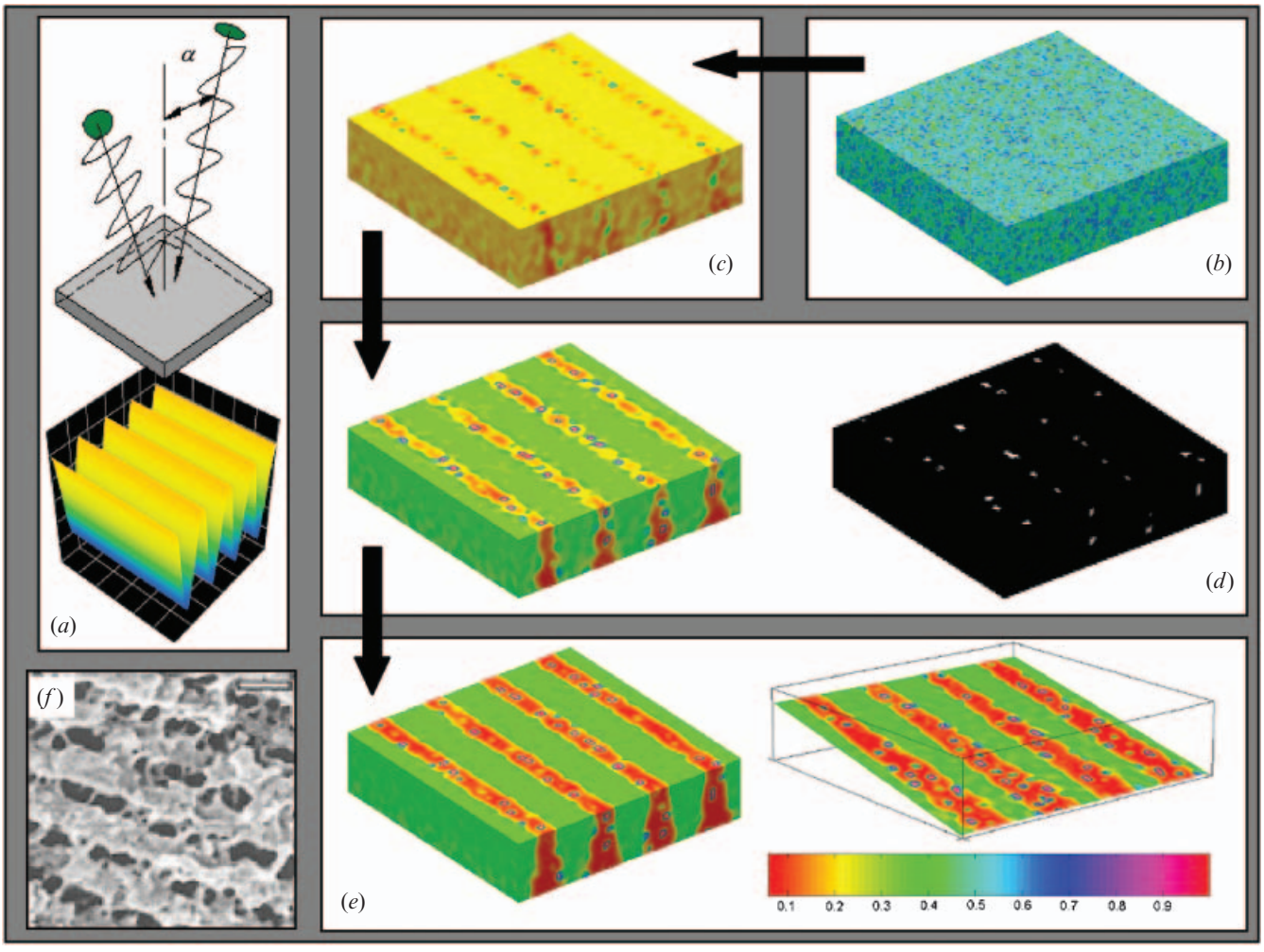

Figure 3. Spatio-temporal evolution of LC volume fraction for the two-beam interference configuration: (*a*) geometric arrangement of light beams and the corresponding irradiance figure (bright regions represent high intensity); (*b*) snapshot at 0 time steps; (*c*) 3 000 time steps; (*d*) 4 000 time steps, concentration order parameter (left) and orientation order parameter (right); (*e*) 5 500 time steps with slice of the lattice demonstrating the effect of attenuation; (*f*) experimentally observed scanning electron micrograph of fringe morphology (scale bar denotes 150 nm).

reciprocal of grating spacing, $1/d_s$, which has been substituted according to Bragg's Law:

$$\frac{1}{d_s} = \frac{N_x}{L} = \frac{2\pi \sin\alpha}{\lambda} \tag{20}$$

where L is the relevant length of the square grid and λ is the wavelength of the incident light, which is selected based on the type of initiator used. As a direct consequence of equation (20), the grating spacing may be controlled by the angle at which the sample is irradiated. The light intensity distribution according to equation (19) is illustrated in figure 3 (*a*), where bright regions correspond to regions of high intensity and darker regions to lower intensities.

The rate constant, k, contains information concerning the spatial distribution of the light intensity through the following relation:

$$k = \frac{k_p}{k_t^{1/2}} (\Phi I)^{1/2} \tag{21}$$

where k_p and k_t represent the individual reaction kinetic constants for propagation and termination since the reaction is free radical in nature. Φ is often referred to as the quantum yield for radical initiation. I corresponds to the absorbed light intensity. It is worth mentioning that, as shown by photo-differential scanning calorimetry (P-DSC) and Fourier transform infrared spectroscopy (FTIR) experiments, k actually decays with elapsed time after the initial spike. In the present computations, the overall typical rate constants gathered from actual experiments were used. To couple the illumination intensity with the reaction-diffusion equations presented in the preceding section, equations (17), (19) and (21) are combined to yield:

$$\frac{d\alpha}{dt} = k \cos\left(\frac{2\pi N_x}{L} x\right)(1-\alpha). \tag{22}$$

Equation (22) is lastly substituted into equations (3) and (4). At this point, numerical solution of the equations governing the concentration and orientation order parameters is possible.

To examine the dynamics of pattern photopolymerization-induced phase separation, the simulation has been conducted under the following conditions: $\phi_{LC}=0.35$, $T=30^\circ C$, $N=4$, $L=120$, $I_0=1$, and $k=2\times10^{-3}\,s^{-1}$. The temperature has been selected such that the mixture initially resides in the isotropic region of the phase diagram before polymerization is initiated, see figure 1 (*a*). The Flory–Huggins interaction parameter, χ, may be estimated from the relation $\chi=A+B/T$, where T is in absolute units, with $A=-10$ and $B=3\,600$ as discussed in earlier works [43]. Our choice of LC volume fraction is based on the experimental findings. In the simulation, we utilized the rate constant k determined experimentally by our group on a tetracrylate monomer cured with the Rose Bengal photoinitiator [47], which is activated upon exposure to green light ($\lambda=532$ nm). To facilitate the simulation procedure, we non-dimensionalize the spatial and temporal variables in the following manner: $\tau=(D_{re}/l^2)t$, $\tilde{k}=(l^2/D_{re})k$, $\tilde{x}=x/l$, and $\tilde{y}=y/l$, where l is the characteristic length scale and D_{re} is the reference diffusion coefficient for the system. The experimental self-diffusion coefficient of liquid crystal is known to be of the order of $10^{-7}\sim10^{-8}\,cm^2\,s^{-1}$, while that of the acrylate monomer is of the order of $10^{-10}\sim10^{-11}\,cm^2\,s^{-1}$ [48, 49]. Therefore, the reference diffusion coefficient is taken to be the average for the mixture, of the order of $10^{-8}\,cm^2\,s^{-1}$. On the other hand, the characteristic length of the system l_c is chosen to be 50 nm, such that the real space dimensions of the cubic lattice are $6\times6\times1.5\,\mu m^3$. The renormalization renders a dimensionless rate constant $\tilde{k}=7\times10^{-7}$ and self-diffusion coefficients of 2 and 0.01 for the LC and monomer, respectively. In regard to relating simulated time steps back to the real space, $t=0.0025\tau$.

Figure 3 (*b–e*) illustrates the spatiotemporal evolution of the LC concentration field during the course of the simulation. The initial morphological snapshot at $\tau=0$, figure 3 (*b*), represents random fluctuations in the initially miscible mixture imparted by the noise term. The pattern of anticipated fringes emerges with appreciable concentration fluctuations at 3 000 time steps, shown in figure 3 (*c*), characterized by the diffusion of the LC species to the regions of low light intensity within the sample. The phase separation is driven by the instantaneous increase in the molecular mass of the polymer, so that the two-phase region of the phase diagram moves upwards, thrusting the system into an immiscibility region, see figure 1 (*b*). Since a characteristic of free radical polymerization is the rapid production of high molecular mass polymer, the thermodynamics of the system probably changes very little after the initial exposure to radiation, and the pattern formation is a diffusion-controlled phenomenon. As witnessed in previous studies [22, 25, 41], the orientation order parameter of the LC phase lags that of the concentration field since a critical concentration of LC molecules is required for the nematic phase to emerge, and thus nematic ordering first appears at 4 000 time steps when adequate LC molecules diffuse into the LC-rich droplet regions. The concentration and orientation order parameters corresponding to this time are displayed in figure 3 (*d*), in left and right columns, respectively. The regions of low intensity do not contain uniform stripes of LC, but rather a dispersed

Downloaded At: 15:58 25 January 2011

droplet-type morphology. The regions surrounding the droplets are very low in LC content, a direct consequence of the diffusion. On the other hand, significant levels of LC are trapped within the regions of high intensity before they can migrate out, again due to the rapid nature of the photo-polymerization, as evidenced by experimental results [11]. Diffusion of neighbouring LC in the low intensity fringes contributing to the growth of the LC-rich droplets continues until the pattern is fixed at 5 500 time steps; the entire lattice and a diagonal slice is depicted in figure 3 (*e*). The final average size of the droplet structures are of the order of a few hundred nanometers after renormalization to real length scale, which is within the reported range of others [11, 12, 50, 51], and also in good agreement with the experimentally observed grating from scanning electron microscopy shown in figure 3 (*f*). Furthermore, in real time, the final simulated pattern has developed in around 14 seconds.

An additional feature demonstrated in the snapshots of figure 3 is the effect of attenuation, or alternatively speaking, the light intensity variation along the thickness due to absorption by the material. As the simulated sample thickness is quite small, as well as those prepared from experiments (of the order of 5–25 μm), absorption is probably not as great an issue as diffraction and scattering, especially in the early stages of the process when the blend is in the single-phase region, but is shown here for the sake of completeness. However, as phase separation proceeds and heterophase structure arises, the absorption may become increasingly important with time. The light intensity attenuation may be described by the Lambert–Beer Law as follows:

$$I(p) = I(0)\exp(-\gamma \mathrm{p}) \tag{23}$$

where γ is the absorption coefficient and p is the path of light through the sample, equal to $z/\cos\alpha$. Now I may be rewritten as

$$I(z) = I_0 \exp\left(-\frac{\gamma z}{\cos\alpha}\right) = I_0 \exp(-\gamma_{\mathrm{eff}} z). \tag{24}$$

In this work, we have taken $\gamma_{\mathrm{eff}} = d_{\mathrm{m}}\phi_{\mathrm{m}} + d_{\mathrm{p}}\phi_{\mathrm{p}} + d_{\mathrm{LC}}\phi_{\mathrm{LC}}$, where d is the optical density and ϕ the volume fraction of each species. The attenuation may be accounted for by incorporating equation (24) into the reaction rate equations. As most prominently demonstrated in the slice of the lattice in figure 3 (*e*), the sample is irradiated on the upper face, and the intensity diminishes slightly while progressing downward so that the fringes become widened and washed out. Loss of the pattern may be witnessed in the case of thick samples and/or with the employment of beams of low intensity.

3.3. *Examination of liquid crystal concentration effects (four-beam interference)*

It is known, both experimentally and theoretically [44, 45], that the LC content affects the final morphology during H-PDLC formation via two-beam interference. It is of particular interest to examine how variations in the LC content affect the final morphology of H-PDLC materials in case of four-beam interference. Using another interference configuration, namely the four-beam scheme, where two sets of two-beams are positioned, separate from each other, on the same side of the sample at an angle α from the normal to the sample surface. As shown in figure 4 (*a*), the emerged morphologies may be best analysed by examination of point defects. The irradiance figure generated by this configuration is depicted in figure 4 (*b*), where the structures thus fabricated are essentially two-dimensional photonic crystals as periodicity is maintained in both the x- and y-directions. Again, the bright areas of the irradiance figure represent regions of high intensity. In this case, the spatial variations in light intensity are represented by the following equation:

$$\frac{I}{I_0} = 4\left[\cos\frac{N_x}{L}x + \cos\frac{N_y}{L}y\right]^2 \tag{25}$$

where N_x/L and N_y/L represent the inverse of periodicities in structure in the x- and y-square lattice, respectively. Equations (17), (21) and (25) require combination such that the spatially-dependent reaction rate equation is deduced, following the procedure presented in the preceding section. For this set of computational results, the same parameters were used as previously employed.

We begin the analysis by examining the mixture containing $\phi_{\mathrm{LC}} = 0.2$. A snapshot of the morphology taken at 6 000 simulated time steps is shown in figure 4 (*c*), where at first glance, the structure appears well defined with cylindrical columns of presumably high LC content embedded in a polymeric matrix. However, further inspection of this morphology by plotting the LC volume fraction vs. axial position down the centre of one of the rows of cylinders along the top of the lattice, shown also in figure 4 (*c*), reveals a different story. As the 0.2 LC content is far from the critical concentration of 0.5, the system is initially stable against phase separation, and the upward progression of the phase diagram with increasing molecular mass of the polymeric component barely envelopes the stationary system point, so that the mixture may be regarded as metastable, even at high conversions of polymer. This effect is demonstrated by inspection of the LC content of the dispersed cylindrical domains, which contain

Downloaded At: 15:58 25 January 2011

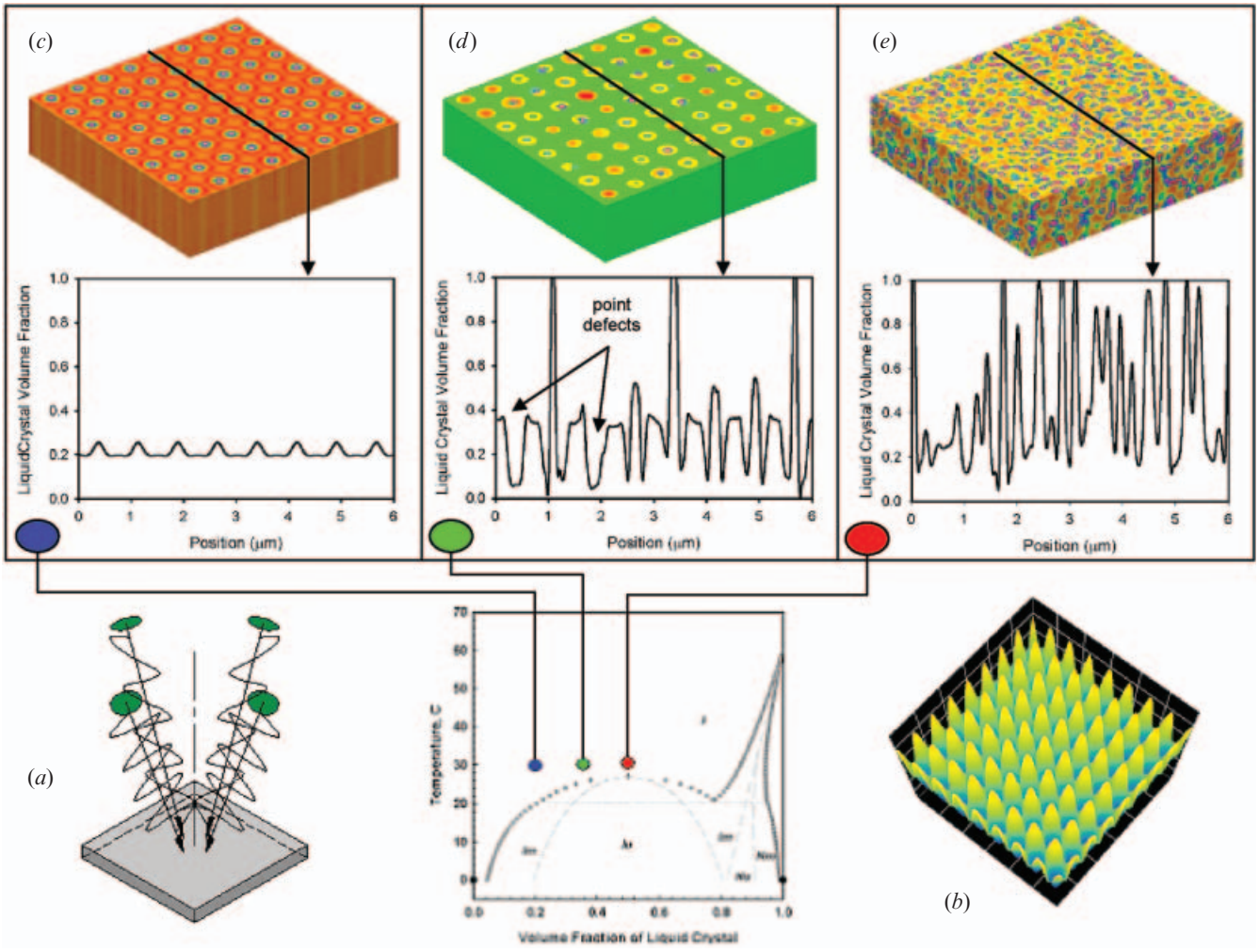

Figure 4. Effect of LC volume fraction on the final morphology of H-PDLC materials using the four-beam interference configuration: (*a*) geometric arrangement of light beams; (*b*) corresponding irradiance figure (bright regions represent high intensity); (*c*) snapshot of morphology at 6 000 simulated time steps for $\phi_{LC}=0.2$, and plot of LC volume fraction vs. axial position extracted from lattice, down the centre of LC domains along *y*-direction; (*d*) structure at 12 750 time steps for $\phi_{LC}=0.35$, and plot of LC volume fraction vs. axial position at same location; (*e*) structure at 6000 time steps for $\phi_{LC}=0.5$, and plot of LC volume fraction vs. axial position again at same location.

approximately $\phi_{LC}=0.3$, not much above the initial concentration of the blend. The level of LC within these domains has certainly not reached the concentration necessary for nematic ordering to occur, rendering an ordered structure which may not be useful in actual photonic applications. Slightly higher amounts of LC could possibly have migrated into regions of low intensity were it not for the decreasing mobility of the system, which is unlikely to be adequate for nematic ordering to take place.

Increasing the LC content exerts a positive effect on the final morphology of the photonic crystal, as witnessed in figure 4 (*d*) where an initial concentration of 0.35 has been used. A snapshot of the structure at 12 750 time steps is displayed along with an extracted plot of LC concentration vs. axial position along the centre of one of the columns on the top of the lattice. The mixture containing 0.35 LC content is much closer to the critical point as witnessed in the reference phase diagram of figure 4, such that as the immiscible region expands upon polymerization, the system point is quickly engulfed into the unstable two-phase region, causing phase separation at much earlier times in comparison with the 0.2 LC mixture. The axially dependent concentration plot demonstrates that the level of LC within the dispersed columns has surpassed far beyond the required level for nematic ordering to occur, thus a feasible photonic crystal has been obtained. The high LC content of the cylinders is attributed to the depth the system has been quenched

Downloaded At: 15:58 25 January 2011

into the immiscible region of the phase diagram with the progression of polymerization. Although a tunable photonic crystal has been achieved, it may be noted that the structure contains several point defects where inadequate levels of LC have migrated into the regions of low intensity. This is strictly a local diffusion problem and will be addressed in the subsequent section.

The last concentration to be examined is that pertaining to the critical volume fraction of the starting mixture, i.e. $\phi_{LC}=0.5$. The initial mixture is already very close to the two-phase unstable region of the phase diagram at 30°C, and even the slightest increase in degree of polymerization of the polymeric constituent thrusts the system into the unstable region. The resultant morphology reflects this fact, as shown in figure 4 (*e*), where phase separation occurs so early in the process that the spinodal-like structure dominates over the holographic pattern formation. No stratified holographic pattern is discernible in this case, as witnessed by the extracted plot of LC concentration vs. axial position, since the system has segregated so strongly via spinodal decomposition.

3.4. *Investigation of the effects of network elasticity on the pattern formation process*

Up to this point, we have excluded the network elasticity term from the formulation of the free energy because of its minor influence on the phase diagram, especially at low LC concentrations. However, one cannot ignore the possibility that it can exert some effect on the holographic pattern formation process and thus the local elastic free energy term is included in the total free energy description. The form of the elastic free energy presented in equation (14) effectively describes the swelling of the crosslinking polymer, contributing positively to the overall free energy of the system. The elastic free energy density is plotted in figure 5 (*a*) as a function of both network species and volume fraction ϕ_P, as well as r_c, which is, as previously described, the segment length between two crosslink points. As polymerization advances, r_c decreases since the network densifies as reactive sites are consumed. As the network increases in density, the elastic free energy contribution increases, which is intuitive since it is more difficult for other species to continue to reside in the network. The effect of ϕ_P on the function is also pronounced, exhibiting a maximum at a concentration of 0.5, which may be described as a balancing effect between the volume fractions of the network and resident constituent phases. A comparison between the elastic free energy density contribution and that of its isotropic counterpart, described by the Flory–Huggins theory, is offered in figure 5 (*b*). The curves correspond to the final state of the reacted polymer in our simulation, i.e. $N_P=1000$ and $r_c=3$. The elastic part is diminutive in comparison with that of the free energy of isotropic mixing; however, this fact may be quite misleading as its implications on the simulated results turn out to be profound.

Figures 5 (*c*, *d*) reveal the difference between the simulated final morphology of H-PDLC materials without/with elastic free energy contribution for the $\phi_{LC}=0.35$ mixture. Close examination of the final morphology in figure 5 (*d*) reveals that the photonic crystal contains virtually no point defects, contrary to the structure produced devoid of network elasticity in figure 5 (*c*). Another important feature of these simulated results is that the final snapshot, taken at 3 000 time steps, requires less than a quarter of the time for the pattern to fully develop in figure 5 (*c*). In the latter case, the pattern develops more rapidly by virtue of the inherent nature of the free radical polymerization, where the crosslinking of the polymer network takes place at early times, driving the system to become more immiscible. The rejected LC molecules tend to accumulate more quickly in the low intensity region, thereby expediting the formation of LC columnar arrays faster and more complete with fewer defects.

Although the elastic free energy contribution does not grossly raise the overall free energy, the enhancement of the immiscibility gap is enough to create the observed regularity of the columnar arrays. It should be cautioned that if the elastic free energy contribution were excessively large, the system would expedite macroscopic phase separation so much so that it dominates over the holographic patterning process, and thus holographic patterning may not be realized as demonstrated in the $\phi_{LC}=0.5$ mixture. On the other hand, the addition of the elastic free energy at very low LC concentrations is extremely small such that the $\phi_{LC}=0.2$ mixture cannot be patterned effectively.

3.5. *Variations in beam configuration*

It is an interesting exercise to predict other possible types of photonic crystals fabricated by utilizing various polarized beam configurations. One example is another two-dimensional periodic structure, which may be created through the employment of three beams geometrically arranged 120° apart from each other. This configuration is depicted in figure 6 (*a*), as well as the corresponding irradiance configuration shown in figure 6 (*b*), resulting from the following spatially

Downloaded At: 15:58 25 January 2011

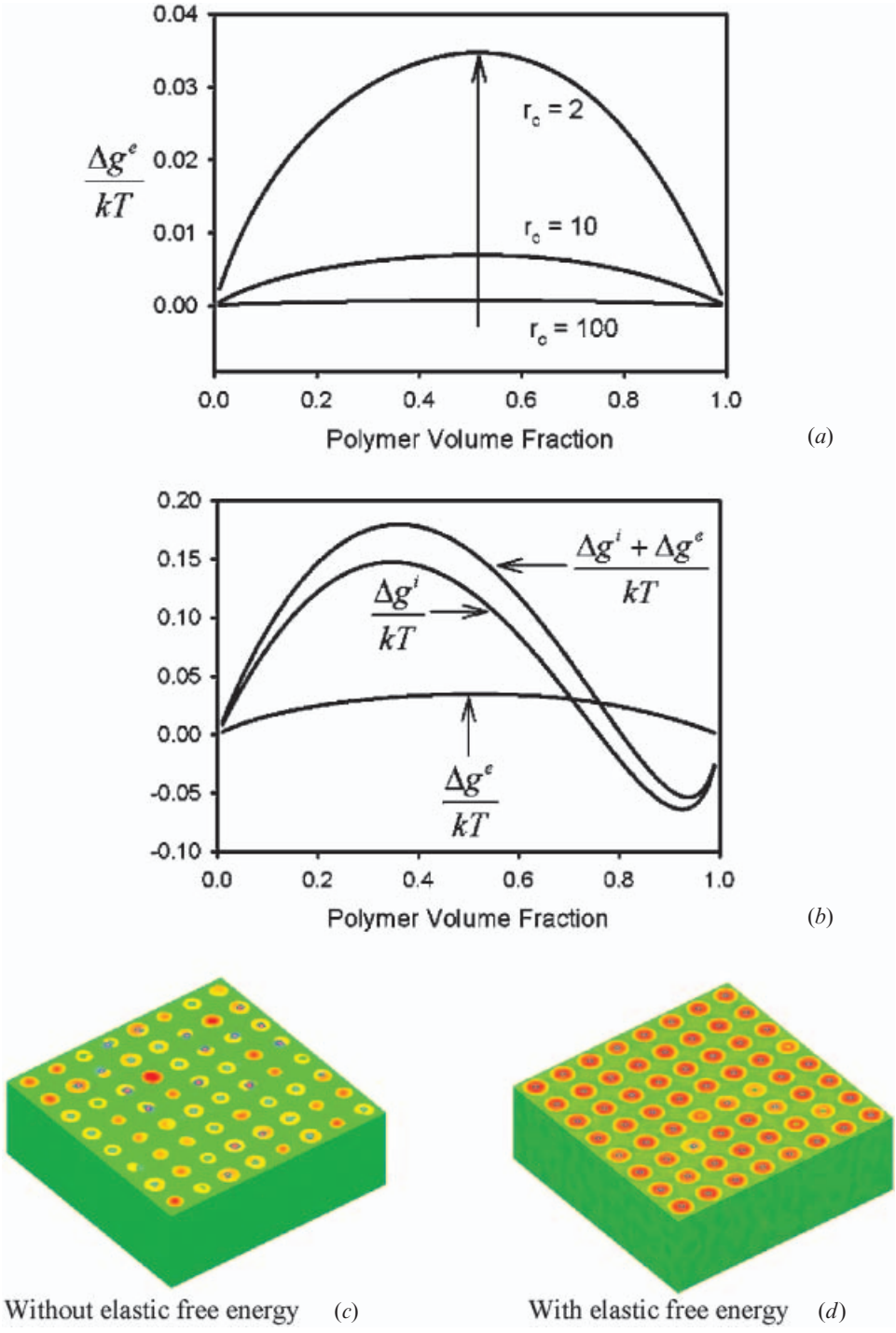

Figure 5. (*a*) Dependence of the elastic free energy density on the polymer volume fraction as well as the distance between crosslink points, which decreases as polymerization advances; (*b*) comparison of the elastic free energy density with the free energy density of mixing according to the Flory–Huggins theory corresponding to the final state of the cured polymer (N_P=1000, R_C=3); (*c*) simulated final morphology of H-PDLC materials without elastic free energy contribution for the ϕ_{LC}=0.35 mixture compared with (*d*) the morphology with elastic free energy contribution.

Downloaded At: 15:58 25 January 2011

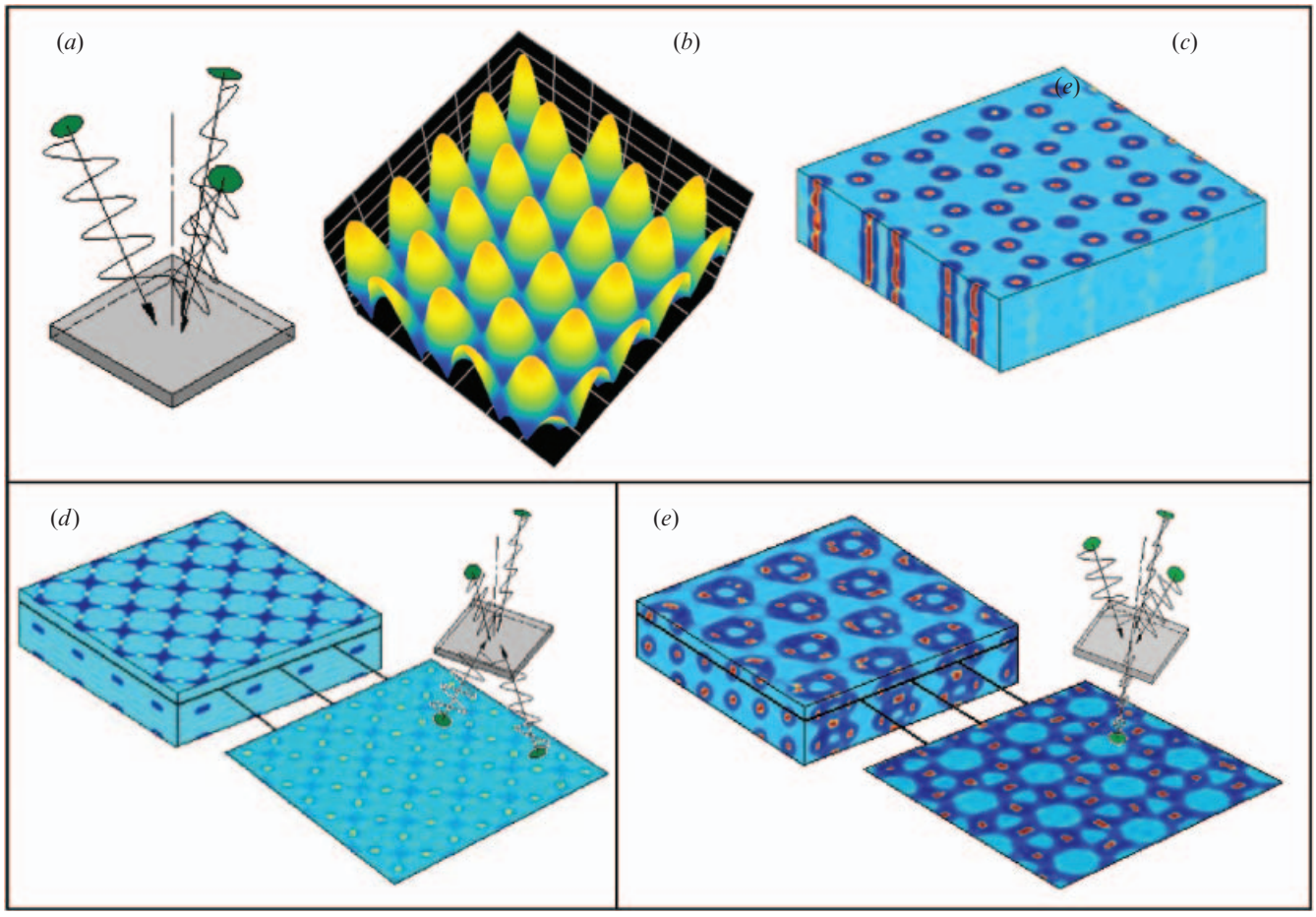

Figure 6. Additional two- and three-dimensional structures: (*a*) representation of the three-beam configuration; (*b*) irradiance figure generated by three-beam interference; (*c*) corresponding two-dimensional hexagonal columnar structure; (*d*) three-dimensional checkerboard pattern via two+two beam interference with slice extracted 375 nm from top surface; (*e*) FCC crystal structure with slice extracted 375 nm from top surface. All morphological snapshots taken at 4 500 time steps.

Downloaded At: 15:58 25 January 2011

dependent intensity equation:

$$\frac{I}{I_0} = 1 + 4\cos\left(\frac{\sqrt{3}N_y}{2L}y\right)\left[\cos\left(\frac{3N_x}{2L}x\right)\cos\left(\frac{\sqrt{3}N_y}{2L}y\right)\right]. \quad (26)$$

The H-PDLC structure resulting from the coupling of this equation with the reaction-diffusion equations yields a hexagonal columnar-type two-dimensional structure, as shown in figure 6 (*c*) taken at 4 500 time steps.

Three-dimensional photonic crystals may be fabricated by irradiating the sample from both sides, employing configurations comprising four polarized beams. In one such arrangement, the two+two beam configuration consists of two beams from above, as well as two from the opposite side. The beams coming from above and below reside in planes perpendicular to each other while those on each side are directed from the opposite directions at some angles to the reflection plane that eventually determine the spacing of the periodic structures. The irradiance pattern resulting from this particular arrangement is described by the following equation:

$$\frac{I}{I_0} = 4\left[\begin{array}{l}\cos^2\left(\frac{N_x}{L}x\right) + \cos^2\left(\frac{N_y}{L}y\right) \\ +2\cos\left(\frac{N_x}{L}x\right)\cos\left(\frac{N_y}{L}y\right)\cos\left(\frac{2N_z}{L}(z-h/2)\right)\end{array}\right] \quad (27)$$

where h represents the sample thickness. The resultant structure from this configuration is demonstrated in figure 6 (*d*), taken at 4 500 time steps. This pattern may be described as a checkerboard type, with alternating layers of ellipsoid shaped LC droplets. To highlight the three-dimensional periodicity, a slice has been extracted from the lattice 375 nm from the top surface, showing that the droplets are rotated 90° from those lying on the topmost layer.

The face-centered cubic (FCC) crystalline structure, which is well known to have the largest inherent

photonic band gap, may also be created via photolithography techniques. The geometric arrangement of the beams in this case is the same as that of the three-wave interference configuration, with the addition of another beam irradiated on the sample, normal to the surface from the opposite side. The irradiance equation derived from this arrangement is as follows:

$$\begin{aligned}\frac{I}{I_0}=4&+2\left[\cos\left(\frac{2\sqrt{2}N_y}{9L}y\right)\cos\left(\frac{N_z}{9L}z\right)\right]\\&+2\left[\sin\left(\frac{2\sqrt{2}N_y}{9L}y\right)\sin\left(\frac{N_z}{9L}z\right)\right]\\&+4\left[\cos\left(\frac{\sqrt{6}N_x}{9L}x\right)\cos\left(\frac{\sqrt{2}N_y}{9L}y\right)\cos\left(\frac{N_z}{9L}z\right)\right]\\&-4\left[\cos\left(\frac{\sqrt{6}N_x}{9L}x\right)\sin\left(\frac{\sqrt{2}N_y}{9L}y\right)\sin\left(\frac{N_z}{9L}z\right)\right]\\&+4\left[\cos\left(\frac{\sqrt{6}N_x}{9L}x\right)\cos\left(\frac{\sqrt{2}N_y}{3L}y\right)+2\cos\left(\frac{2\sqrt{6}N_x}{9L}x\right)\right].\end{aligned}\tag{28}$$

The simulated morphology acquired at 4 500 time steps is demonstrated in figure 6 (*e*), with an extracted slice from the lattice 375 nm from the top surface. The red regions denote high LC content, while dark blue represents areas low in LC. This particular structure has been recently fabricated experimentally from an initial mixture containing 36 wt % LC content, with LC droplets comparable in size to those obtained in our simulation [52].

4. Concluding remarks

We have demonstrated by computational measures several types of photonic crystals, classified by their inherent periodicities as one-, two-, and three-dimensional, which may be fabricated by employing various photolithographic techniques to mixtures of reactive monomer and nematic liquid crystal. Photopolymerization-induced phase separation proceeds as the free energy of isotropic mixing is altered by the increase in degree of polymerization of the polymerizing constituent in regions of high light intensity, forcing the LC species to migrate towards regions of low intensity. Particularly, manipulation of the overall free energy defining the phase diagram allows for the fabrication of optimal structures with few point defects and fast switching response capabilities. The location of the initial mixture on the phase diagram greatly influences the properties of the final morphologies, as it has been demonstrated that blends containing $\phi_{LC}=0.35$ produce crystals with LC-rich domains containing adequate concentrations such that nematic ordering occurs, in accord with experimental observations [47].

We have demonstrated that the addition of the elastic free energy density to the overall free energy formulation exerts profound effects on the pattern formation process, as fully developed patterns occur in less than a quarter of the time than for those devoid of this type of free energy. More importantly, as the fabrication time is already remarkably short, photonic crystals with virtually no point defects are generated when elasticity is accounted for, implying that material selection may be the crucial step in regards to H-PDLC fabrication. Specifically, more flexible network polymers such as hydroxyethyl methacrylate (HEMA), siloxanes, and thiolenes may be preferable to the traditional rigid multifunctional acrylate monomers [53]. It was demonstrated that a rich variety of 3D photonic crystal patterns can be generated upon the manipulation of various beam configurations.

Acknowledgements

Support from the National Science Foundation through Grant # DMR 02-09272, the Collaborative Center for Polymer Photonics, sponsored by Air Force Office of Scientific Research, Wright-Patterson Air Force Base, and University of Akron, Akron Global Polymer Academy, and Ohio Board of Regents Research Challenge Grant is gratefully acknowledged.

References

[1] E. Yablinovitch. *Phys. Rev. Lett.*, **58**, 2059 (1987).
[2] E. Yablinovitch. *Phys. Rev. Lett.*, **67**, 2295 (1991).
[3] T. Zijlstra, E.W.J.M. van der Drift, M.J.A. de Dood, E. Snoeks, A. Polman. *J. vac. Sci. Technol.*, **B17**, 2734 (1999).
[4] P.V. Braun, R.W. Zehner, C.A. White, M.K. Weldon, C. Kloc, S.S. Patel, P. Wiltzius. *Adv. Mater.*, **13**, 721 (2001).
[5] B.H. Cumpston, S.P. Ananthavel, S. Barlow, D.L. Dyer, J.E. Ehrlich, L.L. Erskine, A.A. Heikal, S.M. Kuebler, I.Y.S. Lee, D. McCord-Maughon, J.Q. Qin, H. Rockel, M. Rumi, X.L. Wu, S.R. Marder, J.W. Perry. *Nature*, **398**, 51 (1999).
[6] Y. Fink, A.M. Urbas, M.G. Bawendi, J.D. Joannopoulos, E.L. Thomas. *J. Lightwave Tech.*, **17**, 1963 (1999).
[7] A.M. Urbas, R. Sharp, Y. Fink, E.L. Thomas, M. Xenidou, L.J. Fetters. *Adv. Mat.*, **12**, 812 (2000).
[8] G.M. Whitesides, R. Crzybowski. *Science*, 2418 (2002).
[9] D.J. Broer, J. Lub, C.F. van Nostrum, M.M. Wienk. *Recent Res. Dev. polym. Sci.*, **2**, 313 (1998).
[10] T.J. Bunning, L.V. Natarajan, V.P. Tondiglia, R.L. Sutherland. *Annu. Rev. mater. Sci.*, **30**, 83 and references therein (2000).

Downloaded At: 15:58 25 January 2011

[11] M. Campbell, D.N. Sharp, M.T. Harrision, R.G. Denning, A.J. Turberfield. *Nature*, **53**, 404 (2000).
[12] T.J. Bunning, L.V. Natarajan, V.P. Tondiglia, R.L. Sutherland. *J. polym. Sci. B: polym. Phys.*, **35**, 2825 (1997).
[13] R. Penterman, S.I. Klink, H. de Koning, G. Nisato, D.J. Broer. *Nature*, **417**, 55 (2002).
[14] M. Jazbinsek, I.D. Olenik, M. Zgonik, A.K. Fontecchio, G.P. Crawford. *J. appl. Phys.*, **90**, 3831 (2001).
[15] R.L. Sutherland, V.P. Tondiglia, L.V. Natarajan, T.J. Bunning. *Appl. Phys. Lett.*, **79**, 1420 (2001).
[16] G. Zhao, P. Mouroulis. *J. mod. Opt.*, **41**, 1929 (1994).
[17] S. Piazzolla, B.K. Jenkins. *Opt. Lett.*, **21**, 1075 (1996).
[18] V.L. Colvin, R.G. Larson, A.L. Harris, M.L. Schilling. *J. appl. Phys.*, **81**, 5913 (1997).
[19] H. Nakazawa, S. Fujinami, M. Motoyama, T. Ohta, T. Araki, H. Tanaka, T. Fujisawa, H. Nakada, M. Hayashi, M. Aizawa. *Comput. Theor. polym. Sci.*, **11**, 445 (2001).
[20] S. Piazzolla, B.K. Jenkins. *J. opt. Soc. Am. B*, **17**, 1147 (2000).
[21] J.R. Lawrence, F.T. O'Neill, J.T. Sheritan. *J. opt. Soc. Am. B*, **19**, 621 (2002).
[22] T. Kyu, D. Nwabunma, H.-W. Chiu. *Phys. Rev. E*, **63**, 1802 (2001).
[23] S. Meng, K. Nanjundiah, T. Kyu, L.V. Natarajan, V.P. Tondiglia, T.J. Bunning. *Macromolecules*, **37**, 3792 (2004).
[24] R.L. Sutherland, V.P. Tondiglia, L.V. Natarajan, T.J. Bunning. *J. appl. Phys.*, **96**, 951 (2004).
[25] D. Nwabunma, H.-W. Chiu, T. Kyu. *J. chem. Phys.*, **113**, 6429 (2000).
[26] J.D. Gunton, M.S. Miguel, P.S. Sahni. In *Phase Transitions and Critical Phenomena*, D.C. Domb, J.L. Lebowitz (Eds), Academic Press, New York (1993).
[27] J.R. Dorgan. *J. chem. Phys.*, **98**, 9094 (1993).
[28] H.E. Stanley. *Introduction to Phase Transitions and Critical Phenomena*. Oxford University Press, New York (1971).
[29] M. Takenaka, T. Hashimoto. *Phys. Rev. E*, **43**, R647 (1993).
[30] J.R. Dorgan, D. Yan. *Macromolecules*, **31**, 193 (1998).
[31] Z. Lin, H. Zhang, Y. Yang, *Macromol. Theory Simul.*, **6**, 1153 (1997); Z. Lin, H. Zhang, Y. Yang. *Macromol. Chem. Phys.*, **200**, 943 (1999).
[32] P.G. de Gennes. *J. chem. Phys.*, **72**, 4756 (1980).
[33] P.J. Flory. *J. chem. Phys.*, **10**, 51 (1942).
[34] M.L. Huggins. *J. chem. Phys.*, **9**, 440 (1941).
[35] M. Maier, A. Saupe, *Naturforsch*, **A13**, 564 (1958); M. Maier, A. Saupe. **A14**, 882 (1959); M. Maier, A. Saupe. **A15**, 287 (1960).
[36] C. Shen, T. Kyu. *J. chem. Phys.*, **103**, 7471 (1995).
[37] K. Dusek, *J. polym. Sci., C, polym. Symp.*, **16**, 1289 (1967); K. Dusek, W. Prins. *Adv. polym. Sci.*, **6**, 1 (1969).
[38] H.M.J. Boots, C. Kloosterboer, C. Serbutoviez, F.J. Touwslager. *Macromolecules*, **29**, 7683, 7690 (1996).
[39] F. Benmouna, X. Coqueret, U. Maschke, M. Benmouna. *Macromolecules*, **31**, 4879 (1998).
[40] H.M.J. Boots, J.G. Kloosterboer, C. Serbutoviez, F.J. Touwslager. *Macromolecules*, **29**, 7683 (1996).
[41] B.J. Bauer, R.M. Briber, C.C. Han. *Macromolecules*, **22**, 940 (1989).
[42] P.J. Flory, B. Erman. *Macromolecules*, **15**, 800 (1982).
[43] D. Nwabunma, K.-J. Kim, Y. Lin, L.-C. Chin, T. Kyu. *Macromolecules*, **31**, 6806 (1998).
[44] S. Meng, T. Kyu, L.V. Natarajan, V.P. Tondiglia, R.L. Sutherland, T.J. Bunning. *Macromolecules*, **38**, 4844 (2005).
[45] T.J. Bunning, L.V. Natarajan, V.P. Tondiglia, R.L. Sutherland, D.L. Vezie, W.W. Adams. *Polymer*, **36**, 2699 (1995).
[46] M. Young. *Optics and Lasers*. Springer Verlag, New York (1992).
[47] S. Meng. PhD thesis, University of Akron, USA (2004).
[48] P.G.D. Gennes, J. Prost. *The Physics of Liquid Crystals*, 2nd Edn, Oxford University Press, Oxford (1995).
[49] V. Moreau, Y. Renotte, Y. Lion. *Appl. Opt.*, **41**, 3427 (2002).
[50] R.T. Pogue, L.V. Natarajan, V.P. Siwecki, T.J. Bunning, V.P. Tondiglia, R.L. Sutherland, W.W. Adams. *Polymer*, **41**, 733 (2000).
[51] M.J. Escuti, J. Qi, G.P. Crawford. *Opt. Lett.*, **28**, 522 (2003).
[52] D. Duca, A.V. Sukhov, C. Umeton. *Liq. Cryst.*, **26**, 931 (1999).
[53] L.V. Natarajan, C.K. Shepherd, D.M. Brandelik, R.L. Sutherland, S. Chandra, V.P. Tondiglia, D. Tomlin, T.J. Bunning. *Chem. Mater.*, **15**, 2477 (2003).

Downloaded At: 15:58 25 January 2011